Electronic Supplementary Material (ESI) for Journal of Materials Chemistry C.

Supplementary Information

Synthesis, metal-insulator transition and photoresponse characteristics of VO_2 nanobeams via an oxygen inhibitor-assisted vapor transport method

Xitao Guo[1,†], Yupei Hu[1], Xin Liu[1], Zainab Zafar[2], Weiping Zhou[3], Xingyu Liu[4], Lin Feng[1], Jijun Zou[1], Haiyan Nan[4,†]

[1]Jiangxi Engineering Province Engineering Research Center of New Energy Technology and Equipment, East China University of Technology, Nanchang 330013, China.
[2]Experimental Physics Division, National Centre for Physics, Islamabad 44000, Pakistan.
[3]School of Physics and Materials Science, Nanchang University, Nanchang 330031, China.
[4]Engineering Research Center of IoT Technology Applications (Ministry of Education), Department of Electronic Engineering, Jiangnan University, Wuxi 214122, China.

[*]e-mail: xtguo@ecut.edu.cn (X. Guo) and jnanhaiyan@jiangnan.edu.cn (H. Nan)

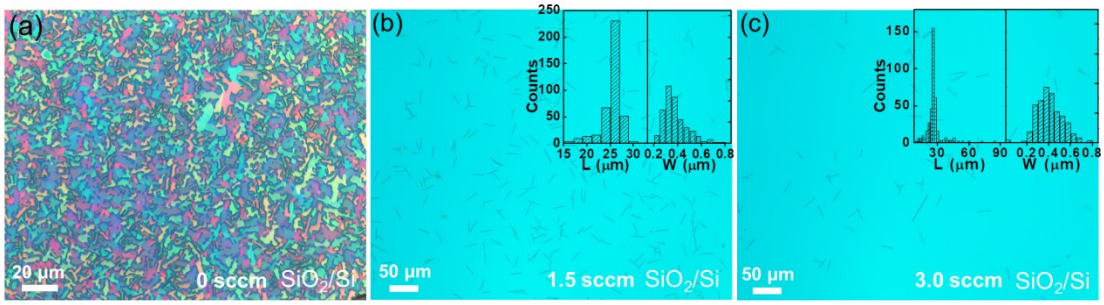

Figure S1. (a-c) The representative OM images of the as-grown VO_2 film and NBs structures observed over the entire substrate for the indicated growth conditions. Insets: the corresponding histograms of the length and width of the VO_2 NBs.

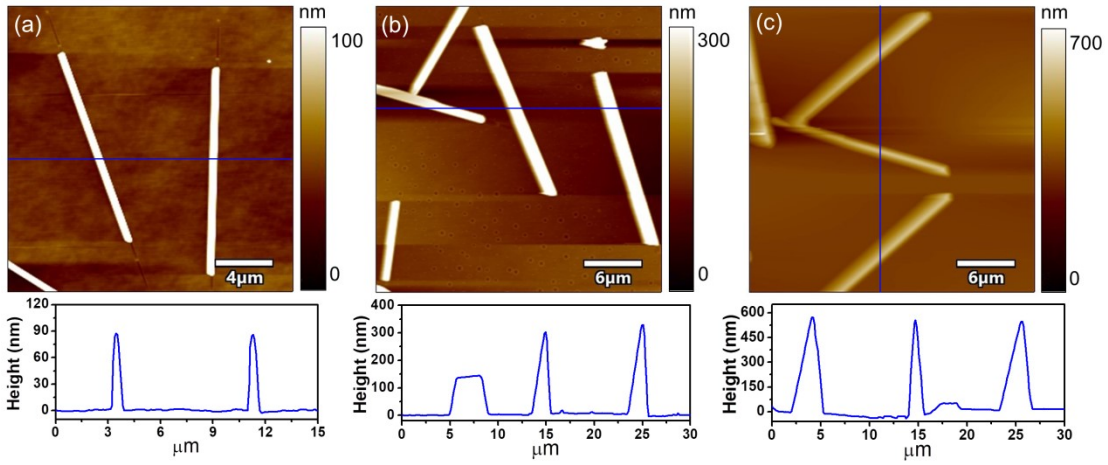

Figure S2. AFM images and the corresponding height profiles of VO_2 NBs on (a, b) SiO_2/Si substrates, and (c) c-cut sapphire substrates. It can see that the thickness of VO_2 NBs on SiO_2/Si substrate is from tens to hundreds of nanometers (roughly 80-350 nm), whereas the VO_2 NBs on sapphire substrate have relatively uniform shapes with thickness up to ~550 nm.

EDS has been used to analyze the elemental composition and distribution of the resulting VO_2 NBs in order to examine the impact of various oxygen levels on VO_2 stoichiometry. Figure S3(a-c) displays all the EDS spectral lines of NBs samples. The insets of Figure S3(a-c) show the relative weight ratio and atomic ratio of O/V in various NBs samples, respectively. As-grown VO_2 NBs have approximately the same stoichiometry due to a slight variation in the O/V atomic ratio, which was calculated to be 2.10, 2.13, and 2.19 under the proposed growth conditions. The most plausible explanation is that all NBs samples experienced prolonged high temperature annealing in step II (900 °C for 300 min, followed by a natural cooling to room temperature only in an argon gas environment). The uniform distribution of O and V elements in VO_2 NBs is demonstrated in Figure S3(d), which depicts a typical elemental mapping of VO_2 NBs at 0.5 sccm O_2.

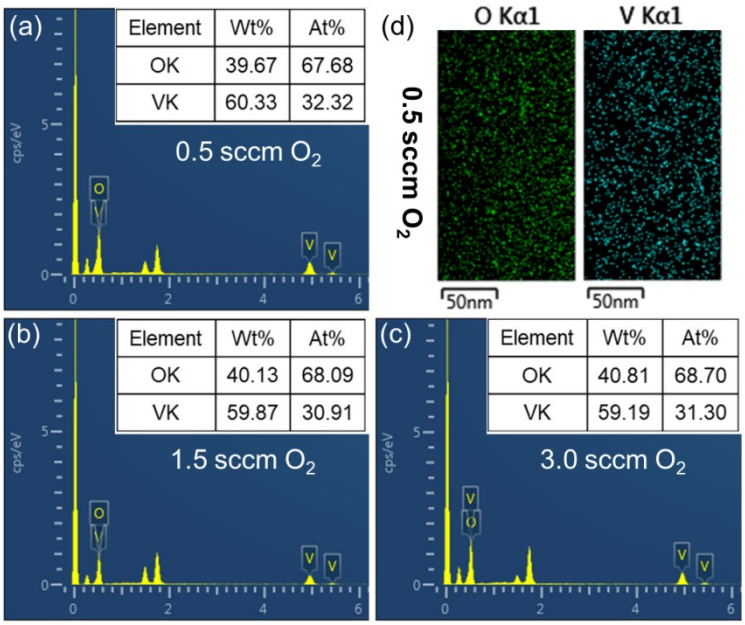

Figure S3. (a-c) EDS spectral lines of the VO_2 NBs grown at different oxygen levels. The insets showing the corresponding elemental composition of different NBs. (d) A typical elemental mapping of VO_2 NBs at 0.5 sccm O_2.

We have also performed the growths of VO_2 NB on c-cut sapphire substrate at different stages, and the corresponding morphologies have been achieved using OM and SEM, as shown in Figure S4(a-d). The crystal morphology evolves from small particle/nuclei to 'V' shaped nanobeam with specific orientation as the increase of the growth temperature.

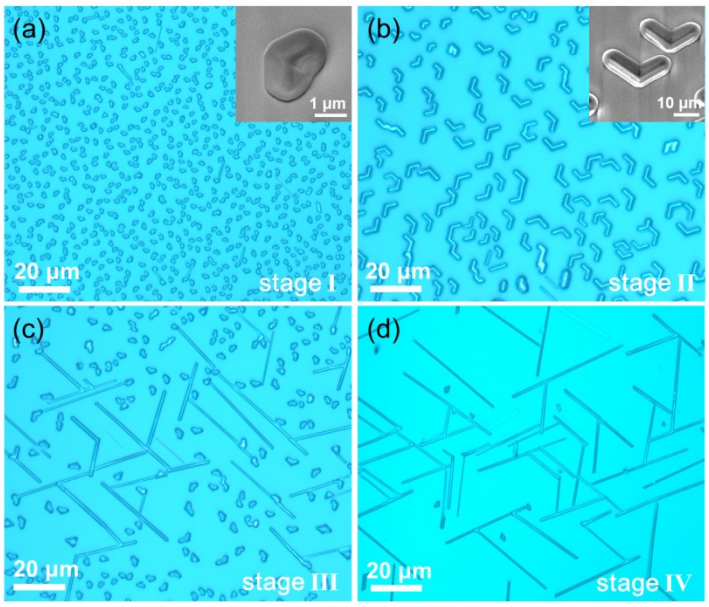

Figure S4. (a-d) Representative OM images of the growth products on c-cut sapphire substrate from the initial stage I to the final stage IV. The insets show the SEM magnified views corresponding to the OM images (a, b), respectively.

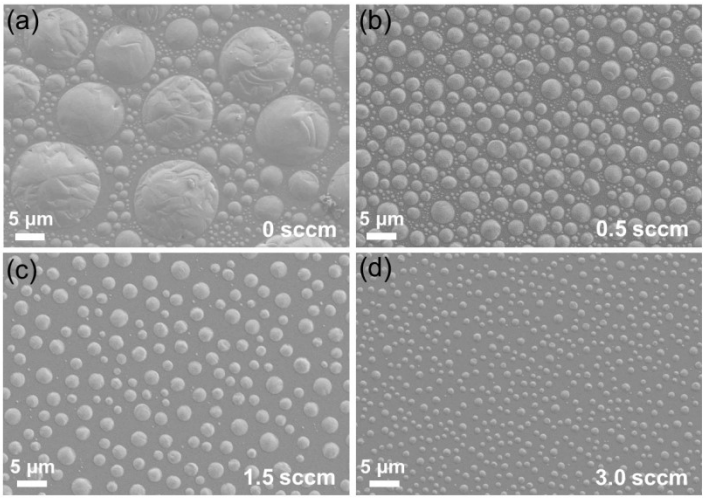

Figure S5. (a-d) SEM images of the V_2O_5 droplets formed on SiO_2 surface for the different O_2 flows at stage I: 0, 0.5, 1.5 and 3.0 sccm, respectively. With the increase of oxygen content, the droplet size decreases significantly from ~10 to ~0.8 μm.

The MIT and photoresponse measurements of VO_2 NBs grown at 1.5 and 3.0 sccm O_2 have also been conducted. Figure S6(a) shows the plots of temperature-dependent resistances of VO_2 NBs grown at different oxygen levels. Although there are some discrepancies in the precise MIT temperature and its hysteresis, all NBs samples display substantial resistance variations with amplitudes up to 5 orders. Based on the aforementioned study, it is possible that the former in our case is primarily driven by the size variances between individual NBs or the sensitivity of MIT to non-uniform substrate adhesion and strain in such end-clamped NBs. Figure S6(b) depicts the relationship between photocurrent and power density for these VO_2 NBs samples when exposed to a 532 nm laser, suggesting that there is no significance difference in the photoresponse characteristics of the devices based on various VO_2 NBs.

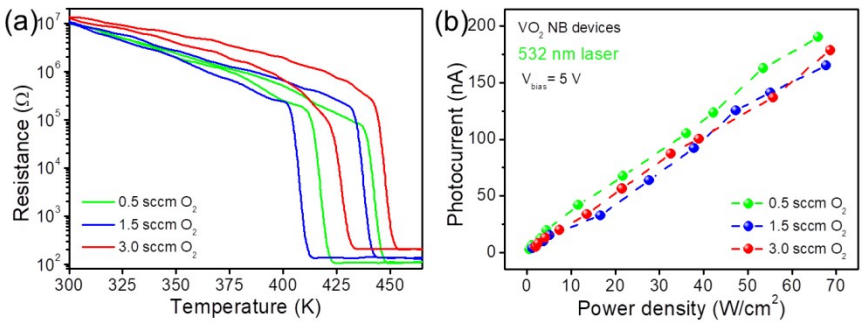

Figure S6. (a, b) Temperature dependent resistance curves and photocurrent versus light density plot of the VO_2 NBs grown at different oxygen levels.

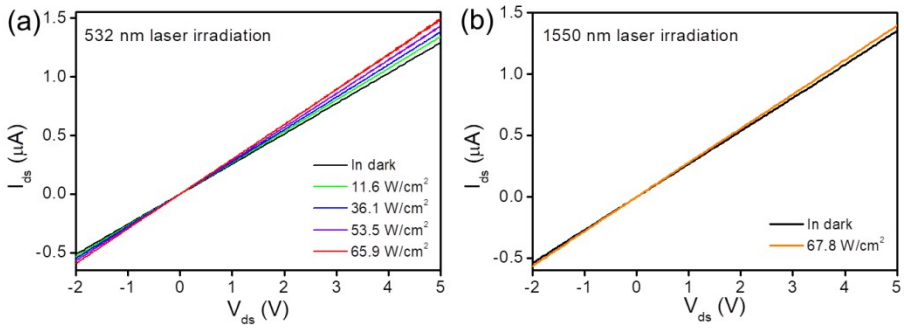

Figure S7. The current-voltage characteristic curves of the device under different wavelengths (532 and 1550 nm) and light intensities.

stage I		stage II/III		stage III/II		stage IV	
145.0	B_{1g}	144.9	B_{1g}	144.0	B_{1g}		
194.1	A_g	195.6	A_g	191.5	A_g	191.2	A_g
		224.9	A_g	221.3	A_g	221.3	A_g
285.1	B_{3g}	284.9	B_{3g}	282.7	B_{3g}		
306.0	A_g	305.8	A_g	306.0	A_g	306.0	A_g
				337.9	B_g	337.9	B_g
				387.1	A_g	389.0	A_g
405.3	A_g	401.9	A_g				
		615.8	A_g	615.6	A_g	612.1	A_g
702.5	B_{1g}	702.3	B_{1g}				
993.9	B_{2g}	993.7	B_{2g}				

Table S1. Summary of the experimentally observed positions of the Raman-active modes of the growth products at different growth stages.

Photodetector	Laser (nm)	V_{bias} (V)	R_λ (mA/W)	Rise time (ms)	Fall time (ms)
VO_2/Si heterostructure[13]	950	0	2×10^{-2}	70	150
VO_2/GaAs heterostructure[14]	980	0	2.5	1.46	1.90
	1310		4.8	1.31	1.58
VO_2/Sb_2Se_3 heterostructure[15]	520	0	244	0.2	0.36
VO_2/ZnO bilayer[16]	365	1	320	2.49×10^3	2.06×10^3
VO_2 thin films/Au[17]	808	1	502.1	138	156
VO_2(M1) thin films[18-23]	1550	10	3.03	1.8×10^2	4.7×10^3
	850	5	16	60	85
	1064	5	40.09	110	160
	1550	10	7.13×10^{-2}	2.23×10^3	3.67×10^3
	1064	10	1.54	1.17×10^3	1.08×10^3
	650	10	~353	1.57	1.64
	980		~78	1.67	4.12
VO_2(B) nanosheet film[24]	405	0.2	9.21×10^3	683	338
VO_2 nanowire[25]	365	5	- (on/off ratio 719)	1.3	4.5
W-doped VO_2 nanowire[26]	532	4	2.15×10^7	4.8	3.9
W-doped VO_2 nanowire array[27]	980	3	21.4	228	206
VO_2(B) nanorods[28]	980	2	-	4.6×10^3	2.8×10^3
VO_2(M1) microwire[29]	360-400	4	7069×10^3	~126	-
VO_2(M1) nanorods[30]	980	2	-	1.6×10^3	1.0×10^3
VO_2/V_2O_5 core/shell NB heterostructure[31]	990	3	2873.7×10^3	50	230
VO_2 NB[32]	800	0.05	$\sim6\times10^{-3}$	-	-
VO_2(M1) NB (This work)	532	5	18	2	7
	1550		3	41	53

Table S2. Comparison of the photoresponse characteristics of our VO_2 NBs photodetector with that of other VO_2 based photodetectors.